Applied Catalysis A: General 347 (2008) 81–88

Contents lists available at ScienceDirect

Applied Catalysis A: General

journal homepage: www.elsevier.com/locate/apcata

Total oxidation of propene at low temperature over Co_3O_4–CeO_2 mixed oxides: Role of surface oxygen vacancies and bulk oxygen mobility in the catalytic activity

L.F. Liotta [a,*], M. Ousmane [b,d,e,f], G. Di Carlo [b], G. Pantaleo [a], G. Deganello [a,b], G. Marcì [c], L. Retailleau [d,e,f], A. Giroir-Fendler [d,e,f]

[a] Istituto per Lo Studio dei Materiali Nanostrutturati (ISMN)-CNR, via Ugo La Malfa 153, 90146 Palermo, Italy
[b] Dipartimento di Chimica Inorganica e Analitica "Stanislao Cannizzaro", Università di Palermo, Viale delle Scienze, Pad. 17, 90128 Palermo, Italy
[c] Dipartimento di Ingegneria Chimica dei Processi e dei Materiali, Università di Palermo, Viale delle Scienze, Pad. 6, 90128 Palermo, Italy
[d] Université de Lyon, Lyon F-69003, France
[e] Université Lyon 1, Villeurbanne F-69622, France
[f] CNRS, UMR 5256, IRCELYON, 2 Avenue Albert Einstein, Villeurbanne F-69622, France

ARTICLE INFO

Article history:
Received 28 April 2008
Received in revised form 29 May 2008
Accepted 30 May 2008
Available online 12 June 2008

Keywords:
Propene total oxidation
C_3H_6-TPR
TPD experiments
Surface oxygen vacancies
SEM characterization

ABSTRACT

Co_3O_4, CeO_2 and Co_3O_4–CeO_2 mixed oxides with Co/Ce nominal atomic ratio 0.1:5, prepared by co-precipitation method with sodium carbonate, were tested in the oxidation of propene under lean condition and the catalyst stability was checked by performing three consecutive heating–cooling cycles. Characterization of the textural properties were performed by surface area measurement BET, X-ray diffraction (XRD) and scanning electron microscopy (SEM) measurements. Among the Co_3O_4–CeO_2 mixed oxides, Co_3O_4 (30 wt%)–CeO_2 (70 wt%) gives the best activity attaining full propene conversion at 250 °C. This sample is characterized by the presence of Co_3O_4 particles well dispersed and in good contact with ceria according to BET and XRD data and as evidenced by SEM micrographs.

Oxygen temperature-programmed desorption (O_2-TPD) and C_3H_6-temperature-programmed reduction (C_3H_6-TPR) experiments were carried out in order to study the surface and bulk oxygen mobility and to correlate it to the activity. At temperature around 200 °C, O_2-TPD experiments showed the desorption of mobile surface oxygen species for the most active samples, Co_3O_4 and Co_3O_4 (30 wt%)–CeO_2 (70 wt%). C_3H_6-TPR experiments for both of the oxides also evidenced a high reactivity at low temperature, especially, for Co_3O_4 (30 wt%)–CeO_2 (70 wt%) giving at 345 °C an intense peak of CO_2 formation.

Conversely, the ceria sample showed by C_3H_6-TPR much less pronounced oxygen bulk mobility, starting to react with propene above 500 °C and forming only CO.

In this case, the catalytic activity of ceria was explained in terms of formation of surface oxygen vacancies which are relevant to the propene oxidation in presence of gaseous oxygen.

1. Introduction

The reduction of air pollution has become an international problem for more than 10 years due to the increasing vehicles and industrial emissions. Volatile organic compounds (VOCs) are recognized as major contributors to air pollution, because of their direct (carcinogenic or mutagen) and indirect effects (ozone and smog precursors) on the environment and health [1]. They are typically found in urban and industrial areas released from power generators, vehicle emissions and solvent employments. According to the Göteborg protocol, the maximum VOC emission level by 2020 in the EU member countries should be reduced by nearly half as compared to the base year 2000 [2].

VOCs include a wide range of compounds, as for example aromatic and aliphatic hydrocarbons, alcohols, ketones, aldehydes, which are easy to oxidize. Therefore, catalytic oxidation of VOCs represents an effective tool for air pollution control [3]. Employed catalysts for catalytic combustion are mainly noble metals, very active at low temperature; however, their use is limited due to the high price, low thermal stability and tendency to poisoning [4]. On the other hand, transition metal oxides are a suitable alternative because of higher thermal stability and lower price [5]. Among transition metal oxides, perovskites, zirconia-based catalysts, manganese and cobalt oxides, have been claimed

* Corresponding author. Tel.: +39 091 6809371; fax: +39 091 6809399.
E-mail address: liotta@pa.ismn.cnr.it (L.F. Liotta).

0926-860X/$ – see front matter © 2008 Elsevier B.V. All rights reserved.
doi:10.1016/j.apcata.2008.05.038

for their effectiveness in VOCs oxidation [6–11]. In particular, Co_3O_4-based catalysts, studied several decades ago for the high activity for CO and VOCs oxidation [12–14], have received again considerable attention in the last years [15–21].

Doping ceria with transition metals is known to modify the redox properties, enhancing the oxygen mobility and improving the catalytic activity [22–24]. High activity of Cu–Ce and Co–Ce mixed oxides in CO and methane oxidation and excellent resistance to water vapour poisoning have been reported [25]. Moreover, physical and catalytic properties of CoO_x–CeO_2 binary systems can be modulated depending on the Co/Ce ratio, preparation method and on the nature of pre-treatments [26–31].

Recently, our group has investigated the methane oxidation activity of Co_3O_4–CeO_2 co-precipitated oxides. The best results have been attained for Co/Ce atomic ratio close to 1 corresponding to the composition Co_3O_4 (30 wt%)–CeO_2 (70 wt%). Highly dispersed Co_3O_4 particles in good contact with CeO_2 with an improved thermal stability and enhanced redox properties were found [32,33]. On these grounds and considering that enhanced VOCs oxidation activity was reported for cobalt oxides reducible at low temperature [18,20], in the present work, the series of Co_3O_4–CeO_2 mixed oxides with Co_3O_4 ranging between 5 and 70 wt%, was investigated for the total oxidation of propene under lean conditions. Propene was chosen as a probe molecule because alkenes are among the major families in automotive exhausts and because of its high photochemical ozone creativity potential (POCP) [34,35]. The attention was focused on the maintenance of the catalyst stability upon three consecutive runs. The activity survey was complemented with C_3H_6-temperature-programmed reduction (TPR) and O_2-TPD experiments. Characterizations by BET, X-ray diffraction (XRD) and scanning electron microscopy (SEM)/energy-dispersive X-ray (EDX) were also performed.

2. Experimental

2.1. Catalyst preparation and characterization

Co_3O_4–CeO_2 composite oxides containing increasing Co_3O_4 loading (5, 15, 30, 50 and 70 wt%, respectively), corresponding to Co/Ce atomic ratio ranging between 0.1 and 5, were prepared by co-precipitation method with sodium carbonate solution (1 M), following a procedure described elsewhere [32]. The obtained materials, labelled as Co*x*Ce (where *x* refers to the Co_3O_4 weight content) were calcined at 650 °C for 5 h (as prepared). Pure Co_3O_4 and CeO_2, prepared by precipitation with sodium carbonate and calcined at 650 °C for 5 h, were used as references.

Specific surface area (SSA) measurements were performed with a Sorptomatic 1900 Carlo Erba Instrument, by physical adsorption of N_2 at the liquid nitrogen temperature, using the BET equation.

X-ray diffraction patterns were recorded with a D 5005 X-ray diffractometer (SIEMENS) using Cu Kα radiation coupled with a graphite monochromator. A divergence slit of 0.2°, a proportional counter and 0.03° step sizes in 2θ were used. The instrumental contribution and the resolution function for the instrumental broadening were calculated using lanthanum boride (NIST). The assignment of crystalline phases was based on ICSD data base (Co_3O_4 no. 24210, CeO_2 no. 28785) [36]. From the line broadening of the main reflection peaks (line 311 for Co_3O_4 and line 111 for CeO_2), particle sizes (d) of the crystalline phases were calculated [37]. The estimated error was ±10%.

Scanning electron microscopy images and energy-dispersive X-ray analyses were obtained on samples upon which a thin layer of gold has been sputtered, using a Philips XL30 ESEM microscope operating in high vacuum at 25 kV.

2.2. Catalytic tests, C_3H_6-TPR and TPD experiments

Catalytic activity tests were performed at atmospheric pressure in a conventional U-shaped fixed bed quartz reactor. The laboratory-made apparatus has been described in details elsewhere [38]. In a typical experiment, the catalyst (200 mg with grain diameters between 50 and 100 μm) was loaded onto a fine-quartz fritted disk and the reaction temperature was continuously monitored by a thermocouple inserted inside the furnace. The reagent gas mixture consisted of 1000 ppm of C_3H_6 + 9% of O_2 in He and the weight hourly space velocity (WHSV) was typically 36,000 mL g^{-1} h^{-1}. The experiments were performed in a temperature-programmed way as follows: heating from room temperature to 500 °C (rate 3.2 °C/min), plateau at 500 °C for 1 h, cooling down from 500 °C to room temperature (rate 1.3 °C/min). This sequence was repeated three times for each sample, obtaining consistent results during all the cycles. To compare the catalytic performance, the third catalytic run was considered for all catalysts and the conversions (%) were calculated on the basis of propene consumption.

The reactants and products (C_3H_6, CO, CO_2 and O_2) were analyzed by gas chromatography, using a dual CTR1column from Alltech (Porapak and molecular sieve) and a TCD for CO, O_2 and CO_2. A Porapak column and a FID were employed for C_3H_6 detection. In addition CO_2 was continuously measured on-line by IR analyser (ROSEMOUNT Binos 1004). The only reaction products were CO_2 and H_2O. Carbon balance was close to ±5% in all the catalytic tests carried out in presence of the gas mixture containing 1000 ppm of C_3H_6 + 9% of O_2 in He.

C_3H_6-temperature-programmed reduction experiments were carried out with the same reactor, by flowing over the sample (200 mg) a mixture of 1000 ppm of C_3H_6 in He, at a flow rate of 120 mL/min. The temperature was increased from room temperature to 1000 °C at a rate of 10 °C/min. At such ramp of temperature the analysis by gas chromatography of C_3H_6 consumption was not useful, therefore, the effluent gases were analyzed only in terms of CO and CO_2 formed by IR detector working in continuous.

O_2-TPD experiments were performed using the same apparatus as for catalytic tests. The catalyst powder, 400 mg, was pre-treated in He by increasing the temperature from 25 to 550 °C (rate 10 °C/min); maintaining the temperature at 550 °C it was oxidized for 30 min by flowing a mixture 5 vol.% O_2 in He (50 mL/min). Then, the sample was cooled down to 25 °C under oxidative atmosphere and, at r.t., was flushed with He for 30 min. The desorption was carried out under He (50 mL/min) by increasing the temperature up to ~1000 °C, following by on-line mass quadrupole (Thermostar™, Balzers) the evolution of oxygen (m/e = 32).

In order to get insight in the reaction mechanism, TPD runs were also carried out over (200 mg) Co_3O_4, Co30Ce and CeO_2 after propene oxidation tests performed at temperatures corresponding to 10% of propene conversion. The reaction was maintained for 30 min, then the samples were cooled down to room temperature under the reaction mixture and, then, flushed by He for 30 min, in order to remove physisorbed species. The TPD analysis was performed under He (50 mL/min) by increasing the temperature up to 1000 °C. The evolution of the species CH_3^+ (m/e = 15), $C_2H_5^+$ and HCO^+ (m/e = 29), O_2 (m/e = 32), C_3H_6 (m/e = 41) and CO_2 (m/e = 44) was followed by mass quadrupole.

3. Results and discussion

3.1. Catalytic activity and textural properties relationship

The catalytic conversion of propene as a function of the temperature, 50–500 °C, is shown in Fig. 1. Co_3O_4 and Co30Ce are

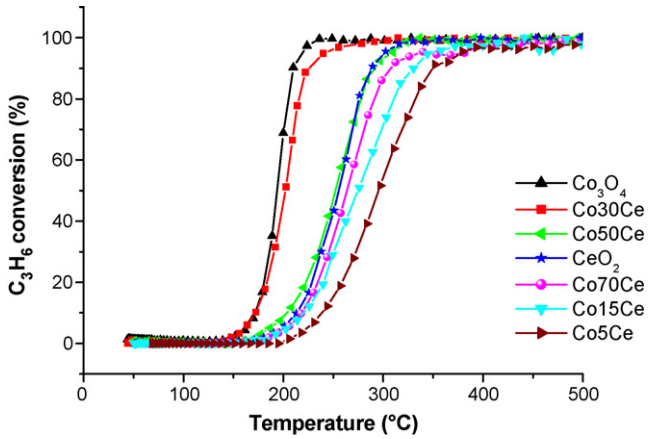

Fig. 1. C_3H_6 conversion (%) over Co*x*Ce catalysts as a function of reaction temperature (°C).

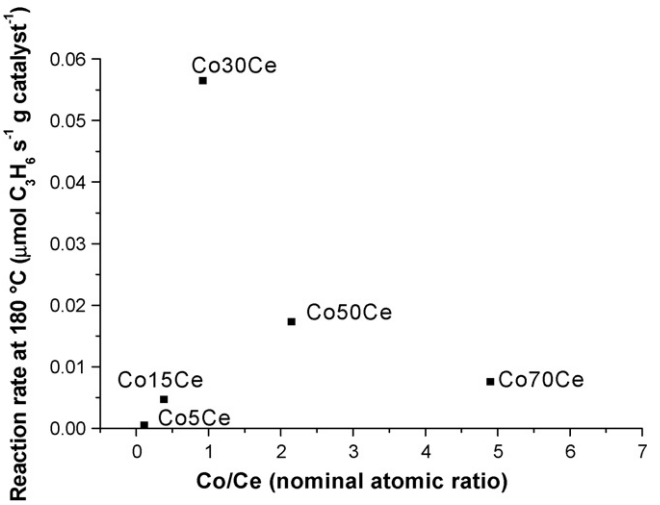

Fig. 2. Reaction rates (μmol C_3H_6 s^{-1} $g_{catalyst}{}^{-1}$) calculated at 180 °C vs. Co/Ce nominal atomic ratio.

Table 1
Temperatures of 20%, 50% and 90% of C_3H_6 conversion during the third reaction run

Sample	T_{20}	T_{50}	T_{90}
Co_3O_4	180	193	210
Co70Ce	232	263	308
Co50Ce	221	250	289
Co30Ce	183	202	225
Co15Ce	239	274	329
Co5Ce	258	295	351
CeO_2	228	254	289

the most active catalysts, then the efficiency decreases in the order: Co50Ce and CeO_2 slightly >Co70Ce > Co15Ce > Co5Ce. However, a thorough analysis of the curves reveals that at low-temperature Co50Ce is more active than CeO_2; Co70Ce and Co15Ce behave similarly at low C_3H_6 conversions (up to around 30%), then for higher values Co15Ce starts to deactivate, reaching the full conversion of propene above 300 °C. Co5Ce behaves as less active in all the conversion range. In Table 1, the temperatures of 20%, 50% and 90% of C_3H_6 conversion in the third reaction run, are listed.

The lowest temperatures were observed with pure Co_3O_4 and Co30Ce, which shows a significant higher activity with respect to pure CeO_2 and to the remaining Co*x*Ce samples. Temperatures of propene conversion during the first and second catalytic runs are close to the values reported in Table 1 (±10 °C).

BET and XRD characterizations of the samples give the same morphological and structural properties previously reported [32], suggesting a perfectly reproducible preparation route. In Table 2 the specific surface area values along with the mean crystallite diameters for the fresh catalysts are listed. According to our previous findings [32], it results that the progressive addition of ceria to cobalt oxide, from Co_3O_4 up to Co5Ce, favours dispersion of Co_3O_4 crystallites and increases the surface area. Unexpected improved textural properties were observed for Co30Ce. In our opinion, this behaviour is due to the peculiar composition (Co/Ce atomic ratio equal to 1) which somehow favours the best interaction between the two oxides.

Characterizations performed over the catalysts after reaction evidenced that no significant sintering occurred upon three consecutive cycles. The specific surface area and mean particles size for the samples after reaction are comparable to the values of fresh samples within ±15%.

Expressing the catalytic results as specific reaction rates (μmol C_3H_6 s^{-1} $g_{catalyst}{}^{-1}$) calculated at 180 °C at which the conversion is ≤20% a more complete image of the effects of Co_3O_4 composition may be obtained. In Fig. 2 the reaction rates versus Co/Ce nominal atomic ratio are plotted. As demonstrated by EDX, the Co and Ce nominal contents for each Co*x*Ce sample are in well agreement with mean values measured on various agglomerates of particles (see Table 3). An inspection of Fig. 2 suggests a volcano-type dependence of the reaction rates versus Co/Ce atomic ratio. By increasing the cobalt content the activity increases correspondingly up to Co50Ce, then decreased with further increase of cobalt content (Co70Ce). The sample Co30Ce diverges from this behaviour, exhibiting significantly higher reaction rate.

In Fig. 3a and b the reaction rates versus the particle sizes of cerium and cobalt oxides phases are displayed. The best performing Co30Ce is characterized by CeO_2 and Co_3O_4 crystallites as low as 14–15 nm, respectively. Then, the rates decrease by increasing the particle diameters. In spite of almost the same d_{CeO_2} value, the samples Co50Ce, CeO_2 and Co70Ce differed in their reaction rates (Co70Ce < CeO_2 < Co50Ce). The higher dispersion of Co_3O_4 particles in Co50Ce with respect to Co70Ce could account for its higher activity, however, it is likely that also other properties may influence the activity.

Table 2
Morphological and structural parameters of Co*x*Ce samples

Sample	SSA (m^2/g)	$d_{Co_3O_4}$ (nm)	d_{CeO_2} (nm)
Co_3O_4	11	72	
Co70Ce	21	43	22
Co50Ce	22	31	21
Co30Ce	33	14	15
Co15Ce	24	n.d.[a]	25
Co5Ce	29	n.d.[a]	28
CeO_2	37		23

[a] Not detectable.

Table 3
EDX data of selected Co*x*Ce samples

Sample	Nominal atomic percentage		EDX atomic percentage[a]	
	Co	Ce	Co	Ce
Co70Ce	83	17	86 ± 2	14 ± 2
Co30Ce	48	52	49 ± 15	51 ± 15
Co15Ce	27	73	28 ± 2	72 ± 2

[a] Mean values.

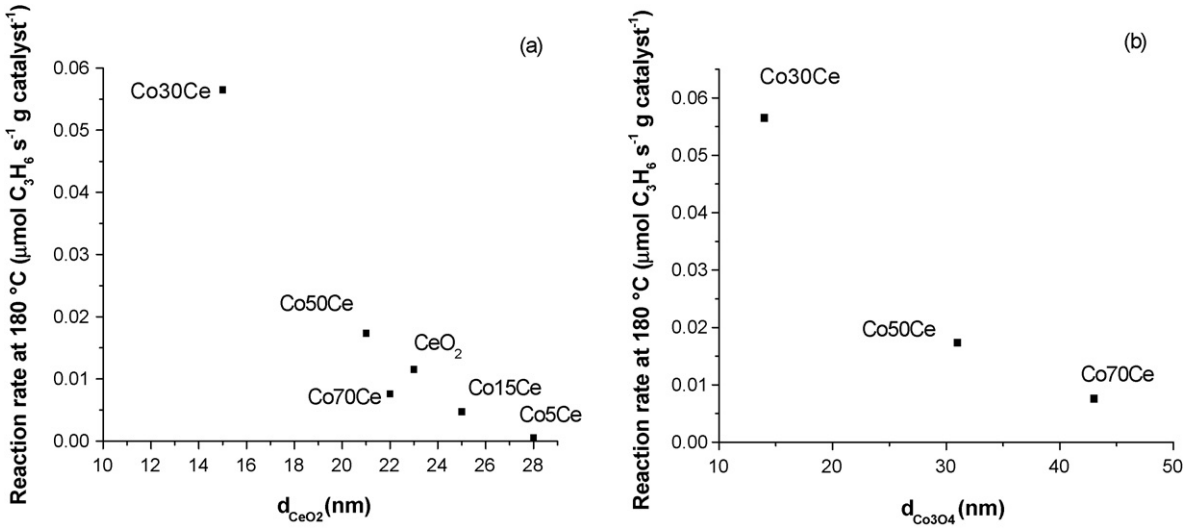

Fig. 3. Reaction rates (μmol C_3H_6 s^{-1} $g_{catalyst}^{-1}$) calculated at 180 °C vs.: (a) d_{CeO_2} (nm) and (b) $d_{Co_3O_4}$ (nm).

Co15Ce and Co5Ce are less active than pure CeO_2 according to the higher ceria particle sizes and lower surface area.

3.2. SEM/EDX characterization

SEM images (Fig. 4) show that all the prepared samples consisted in particles agglomerates. The shape of bare samples, CeO_2 and Co_3O_4, are dramatically different from each other. In particular the CeO_2 sample seems to be constituted of agglomerates of sliver-shaped particles leaving in between big cavities with size in the range 1–5 μm (macroporosity). On the contrary, the Co_3O_4 agglomerates are much more compact and consist in particles with smaller size than those of the CeO_2 sample (75–100 nm). With the mixed samples, it is observed that the shape of the particles changes from the Co15Ce to the Co70Ce. The aspect of the Co30Ce agglomerates is intermediate between that of the Co15Ce and Co70Ce. Moreover, concerning the Co15Ce sample, in which the ceria content is higher, the shape of the particles in the agglomerates are very similar to that of the bare CeO_2 powder. Nevertheless the "slivers" are covered by other particles with shape similar to that of the Co_3O_4 sample. Same considerations can be done for the Co30Ce sample in which the ceria typical sliver-shaped particles are covered by similar particles, to those of the Co_3O_4 sample. From the study of the Co70Ce sample micrographs, it can be observed that their agglomerates consist in very similar particles to those of the Co_3O_4 powder even if they are somehow less compact.

The observed cobalt enrichment of the surface is in agreement with XPS data on similar samples [32] and could be a consequence of the calcination process, at 650 °C, driving the cobalt from the bulk to the surface.

EDX atomic percentages among with the maximum oscillation of the recorded experimental values are listed in Table 3. It is worth noting that the atomic percentages of Ce and Co reported in Table 3 are the average of several values recorded on different agglomerates present in a large area of ca. 500 μm per side. The Co15Ce sample is very homogeneous; in fact, the maximum oscillation of the atomic percentage in this sample is ±2. In this sample, moreover, the average content of both Ce and Co was coincident with the nominal one. In the case of Co30Ce it was observed that the content in Ce is in some cases slightly higher and in others slightly lower on respect to the nominal value. However, the average calculated percentage of Co and Ce considering a very big amount of agglomerates was coincident with the nominal value. Finally, the EDX study of the Co70Ce sample evidenced agglomerates whose cerium content is homogeneous but slightly lower that the nominal one. Summarizing, the samples morphology strongly depends on the chemical composition, in agreement with the trend of structural properties (Table 2). The average percentage of Co and Ce in the Co*x*Ce samples was quite homogeneous, although a slight cobalt enrichment of the catalysts surface was found.

3.3. C_3H_6-TPR and TPD studies

The participation of bulk oxygen ions in the catalytic oxidation reactions over metal oxides has been well established [39] and hydrocarbon oxidations over Co_3O_4 are often reported to occur through a redox mechanism in which the metal oxide reducibility governs the activity [18–20]. Accordingly, our previous results [32,33] highlighted the influence of the enhanced redox properties of Co*x*Ce mixed oxides on methane oxidation activity, as well as recent findings evidenced an increased CO oxidation activity due to the combined effect of cobalt oxide and ceria [26,30].

In order to find a qualitative relationship between the propene oxidation activity and the bulk oxygen mobility, C_3H_6-TPR were carried out on selected samples, Co_3O_4, Co30Ce, Co50Ce and CeO_2. The aim of the experiment was to compare the oxygen reducibility of these catalysts by C_3H_6, therefore, the processes were carried out by using a ramp of temperature of 10 °C/min, a typical rate used for TPR tests. In such conditions the effluent gases were analyzed in terms of CO and CO_2 formed. The resulting profiles are displayed in Fig. 5a–d. Co_3O_4 and Co30Ce are able to oxidize some C_3H_6 to CO_2 at low temperature, showing two CO_2 evolution peaks centred, respectively, at 380 and 460 °C for Co_3O_4 and at 345 and 445 °C for Co30Ce (Fig. 5a and b). CO formation also occurred over both samples above 400 °C. Over Co_3O_4, the CO formation was less important (peak maximum, 1500 ppm, at 530 °C) than the CO_2. On the contrary, Co30Ce showed massive CO evolution (around 2000 ppm) at high temperature with three main peaks at 520, 660 and at 850 °C. Looking at Co50Ce, less active in propene oxidation than both, Co_3O_4 and Co30Ce (Fig. 1), it formed some CO_2 above 400 °C with three main peaks at 440, 510 and at 590 °C, respectively. The CO evolution started above 500 °C and was less pronounced than for Co30Ce (peak maximum, ~1700 ppm, at 715 °C).

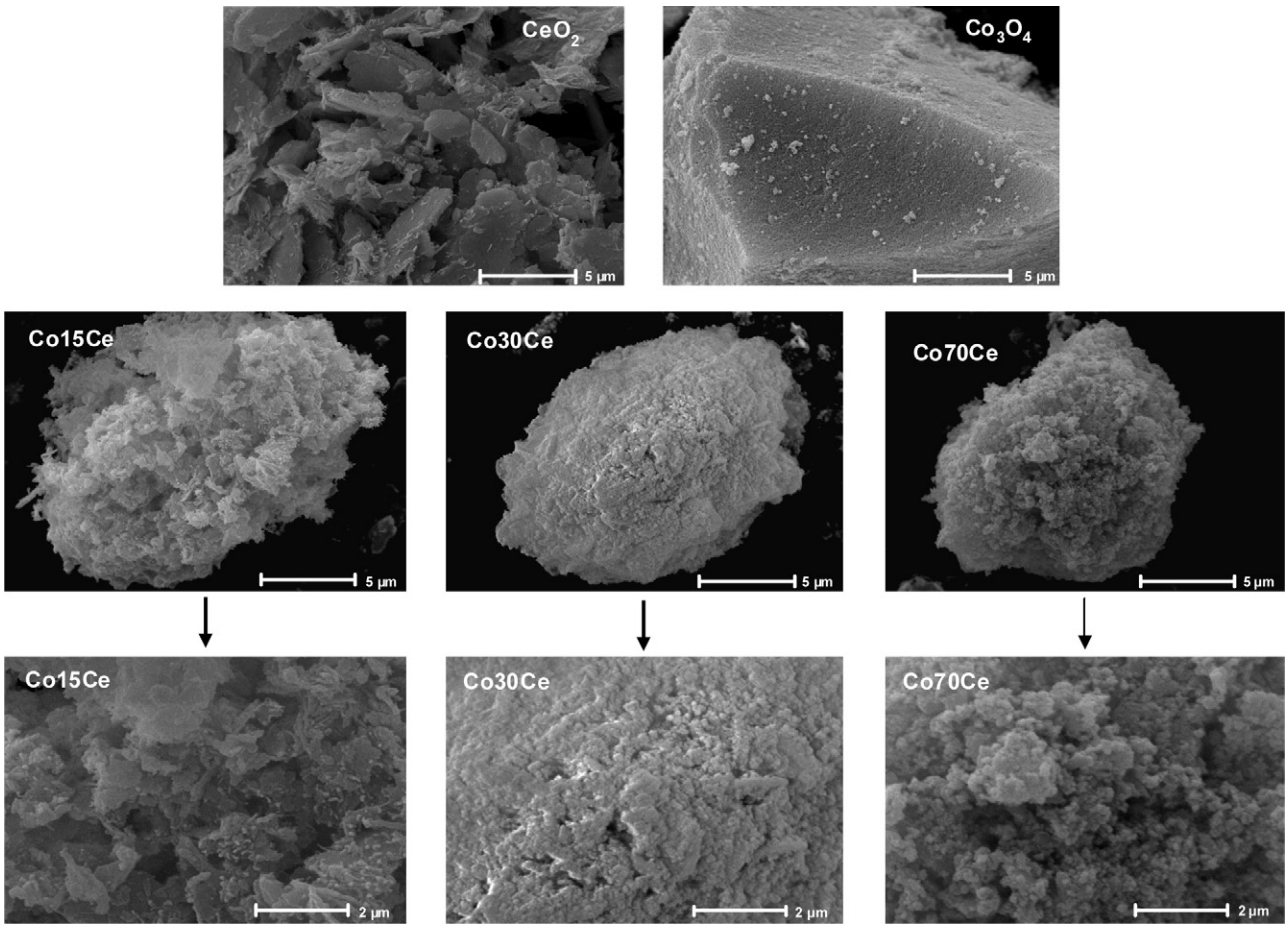

Fig. 4. SEM micrographs of selected Co*x*Ce samples.

On the basis of propene oxidation activity and C_3H_6-TPR over Co_3O_4, Co30Ce and Co50Ce, it results that the higher the CO_2 formation at low temperature, the higher the catalytic activity.

On the other hand, by comparing the CO evolution curves (Fig. 5a–d) it can be surmised that by increasing the ceria content in the mixed oxides increases the CO formation at high temperature. Accordingly, no CO_2 formation was detected for ceria, which gives rise only to CO evolution above 500 °C (Fig. 5d).

To summarize, the highest activity for Co_3O_4 and Co30Ce, better performing than Co50Ce is attributable to their higher reactivity with propene to form CO_2. These findings are in agreement with the relationship found between H_2/CO reducibility of Co_3O_4–CeO_2 mixed oxides and methane oxidation activity [32,33].

It is worth noting that Co50Ce and pure CeO_2 gave similar propene conversion curves above 250 °C (Co50Ce was more active at lower temperature Fig. 1), however, their C_3H_6-TPR profiles were substantially different. Therefore, on the basis of these data, the lattice oxygen mobility of Co_3O_4, Co30Ce and Co50Ce seems important in the propene oxidation, while the activity of ceria should be governed by another mechanism.

The oxidation reactions are known to occur through two possible mechanisms: a suprafacial and/or an intrafacial mechanism [40]. The former mechanism is operative a $T < 400$ °C and involves oxygen species adsorbed over the surface oxygen vacancies of the catalyst. The latter one takes place at $T > 400$ °C and involves the lattice oxygen of the catalyst through a so-called Mars-van Krevelen redox cycle. In the latter case, a direct relation between the catalyst reducibility and the activity takes place.

In order to get further insight in the propene oxidation over Co*x*Ce samples, temperature-programmed desorption experiments were also carried out. Fig. 6a and b show the O_2-TPD curves of the Co*x*Ce catalysts pre-treated with a mixture 5 vol.% O_2 in He at 550 °C. All the samples exhibit a sharp peak of physisorbed O_2 at 50 °C (Fig. 6a), then by increasing the temperature, the desorption profiles change depending on the sample type (Fig. 6b). Co_3O_4 and Co30Ce present below 200 °C a single and well-defined peak with a maximum centred at 160 and 190 °C, respectively. It should be noted that this peak is more intense for Co30Ce. At higher temperature, above 700 °C, a massive oxygen evolution was observed for Co_3O_4 and Co30Ce as well for the others Co*x*Ce oxides, owing to the thermal decomposition of Co_3O_4 to CoO. For Co30Ce, the TPD profile also shows a weak broadened oxygen evolution, below 700 °C. Co70Ce and Co50Ce show similar signals: a small feature at 80 °C, one or two peaks within 150–250 °C, an additional peak around 350 °C, then at higher temperature a peak at 650 °C, just before the thermal decomposition. For Co15Ce only a small feature at 200 °C was observed, while there is no O_2 desorption peak in the TPD profile of CeO_2 in this range of temperature, as previously reported [28]. A small peak was observed above 900 °C.

According to the literature [41,42], in O_2-TPD curves two desorption peaks are usually observed: α and β. The low-temperature peak ($T < 400$ °C), called α, represents the desorption of oxygen adsorbed on the surface oxygen vacancies, such as the species O_2^- and O^- [28]. The high-temperature peak ($T > 400$ °C), called β, is considered as coming from the bulk of the solid. The onset temperature of the β peak, at around 650 °C, is very near to

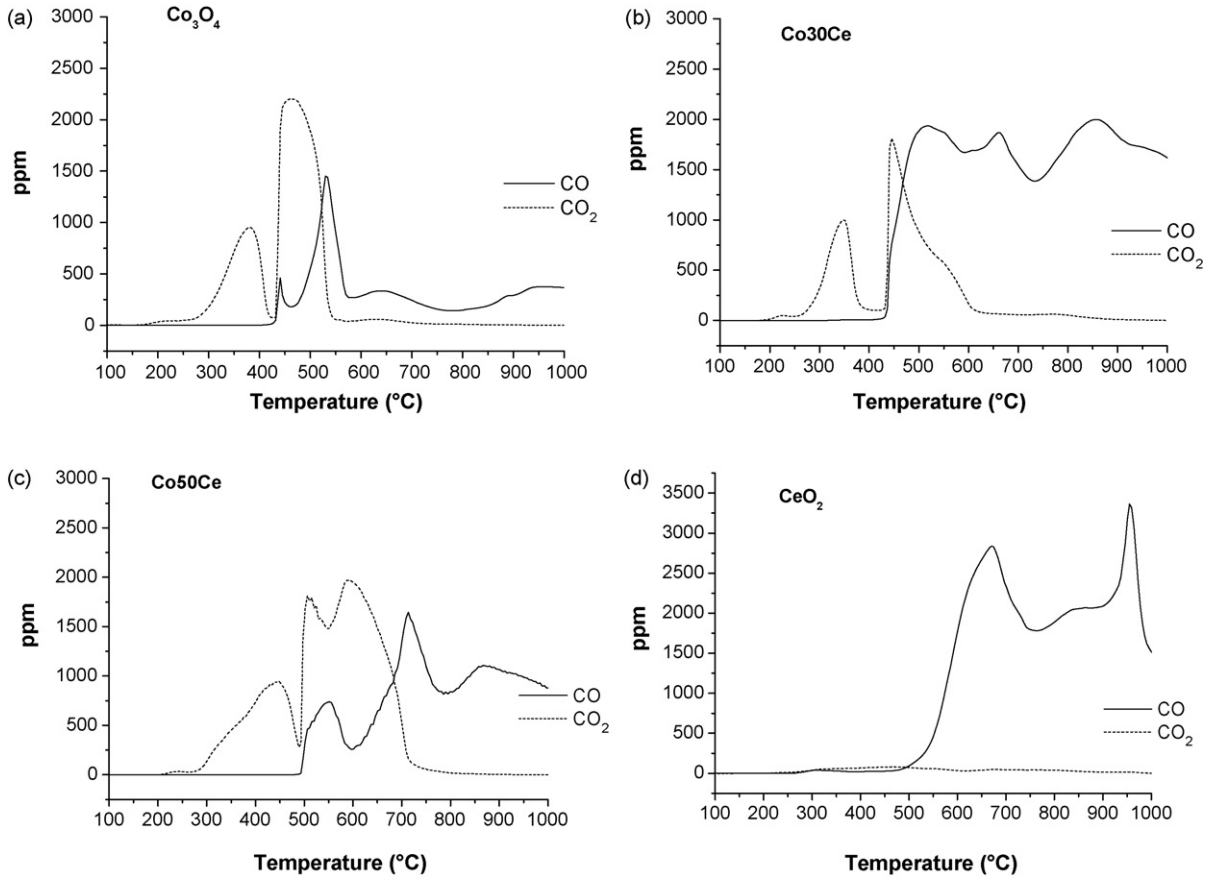

Fig. 5. CO and CO_2 evolution vs. temperature (°C) during C_3H_6-TPR experiments over selected Co*x*Ce samples: (a) Co_3O_4; (b) Co30Ce; (c) Co50Ce and (d) CeO_2.

that of thermal decomposition of the metal oxide, Co_3O_4, that is centred at 800 °C (Fig. 6b). The α-oxygen species are known to participate in oxidation reactions by means of the suprafacial mechanism, while β-oxygens, coming from the catalyst framework, participate to the reaction through the Mars-van Krevelen mechanism [43].

The high mobility of oxygen vacancies on the surface of ceria is well-known [44]. Superoxide (O_2^-) and/or peroxide (O_2^{2-}) species are transiently produced by oxygen adsorption on the surface reduced defects formed under vacuum already at 200 °C or upon thermal treatment at higher temperatures [45]. Such species, not stable when out-gasing or when heated, quickly desorb. Accordingly, we did not observe desorption of O_2 for CeO_2 except for the sharp peak at 50 °C, common to all the samples (Fig. 6a), along with a small feature around 900 °C due to bulk oxygen removal.

Therefore, based on O_2-TPD results, Co30Ce and, to a less extent, Co_3O_4 show a relevant concentration of surface oxygen species, easily desorbed below 200 °C. This type of oxygen is likely to be

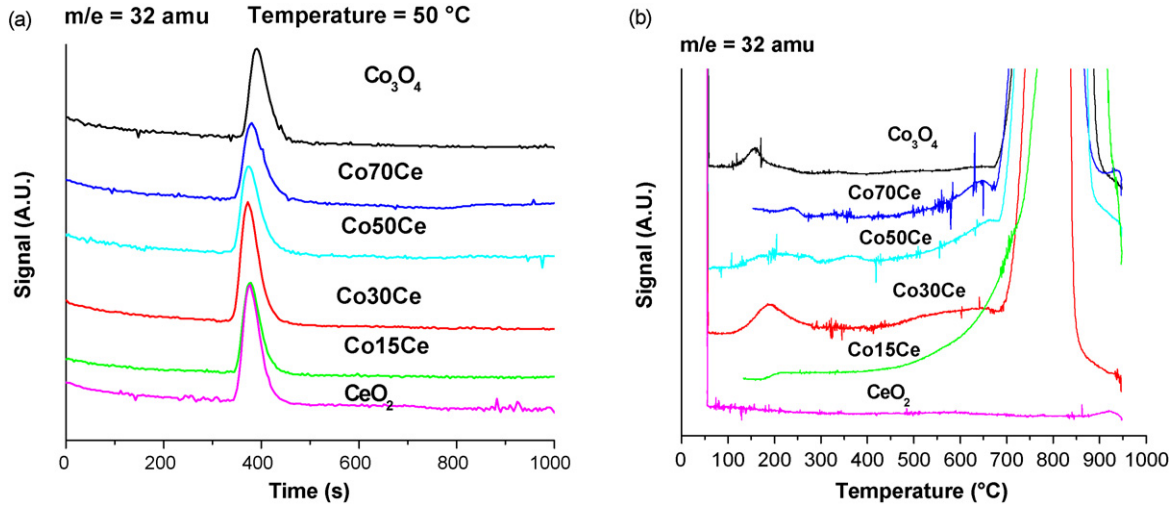

Fig. 6. O_2-TPD curves over Co*x*Ce samples: (a) QMS signal at $m/e = 32$ vs. time (min) at $T = 50$ °C and (b) QMS signal vs. temperature (°C).

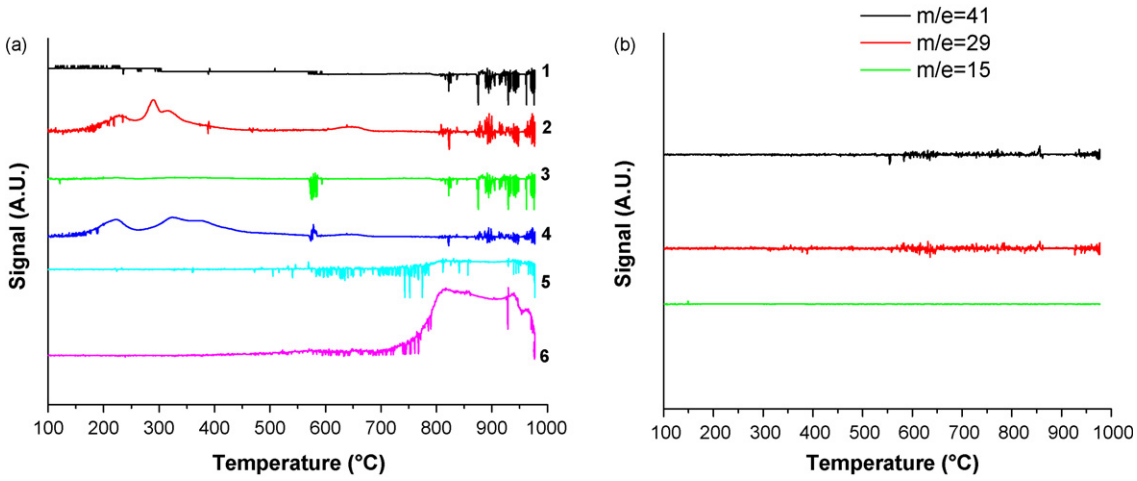

Fig. 7. TPD curves after C_3H_6 oxidation (at temperature giving 10% conversion): (a) QMS signals at m/e = 28 (CO) and at m/e = 44 (CO_2) for Co_3O_4 (curves 1 and 2), Co30Ce (3 and 4) and CeO_2 (5 and 6); (b) QMS signals at m/e = 15 (CH_3^+), m/e = 29 ($C_2H_5^+$/HCO^+), (m/e = 41 (C_3H_6) recorded for Co30Ce. The curves are representative also for Co_3O_4 and CeO_2 samples.

also involved in the propene oxidation, through a suprafacial mechanism. Looking at CeO_2, the presence of oxygen surface vacancies, continuously filled by oxygen from the gas phase, appears in this case the only factor governing the catalytic activity.

The mechanism of interaction between olefin molecules and oxygen at the surface of an oxide catalyst consists of a network of parallel and consecutive steps, leading to different products (selective allylic oxidation or total oxidation), depending on the respective reaction rates [46,47]. Kinetic studies performed on the propene oxidation over Co_3O_4 demonstrated that the reaction leads to the total oxidation to CO_2 through an electrophilic oxidation in which O_2^- and O^- chemisorbed species are involved [48]. Such species are formed over the catalyst surface as the result of a dynamic equilibrium between the gas phase oxygen and the metal oxide. Moreover, previous studies on homomolecular isotopic exchange of oxygen reported an exceptional high rate of exchange on the surface of Co_3O_4 [49].

To get further insight in the propene oxidation process over Co*x*Ce samples, selected catalysts were studied by TPD experiments after reaction at low propene conversion (10%). Fig. 7a shows the desorption features at m/e = 28 (CO) and m/e = 44 (CO_2) over Co_3O_4, Co30Ce and CeO_2 in the range of temperature 100–1000 °C. The propene concentration in the flow was determined from the signal at m/e = 41, while the formation of any species resulting from the hydrocarbon fragmentation and conversion was followed from the signals at m/e = 15 (CH_3^+), m/e = 29 ($C_2H_5^+$/HCO^+) and m/e = 44 (CO_2). The results of oxygen TPD were consistent with those already reported in Fig. 6b and, therefore, were omitted. No C_3H_6, CH_3^+, $C_2H_5^+$/HCO^+ desorption peaks were observed (example given in Fig. 7b for the sample Co30Ce), suggesting that complete propene oxidation to carbon dioxide and water occurred. Co_3O_4 and Co30Ce showed desorption of CO_2 in the range of temperature 180–400 °C, while CeO_2 desorbed CO_2 at much higher temperature ($T > 700$ °C) due to high basicity of ceria surface stabilizing CO_2 as carbonate [45]. The absence of evident CO evolution (Fig. 7a) would be also an indication that propene oxidation occurs without formation of carbon deposit. Indeed, in that case, oxidation of carbonaceous species by Co*x*Ce at high temperature, during the TPD process, would lead to massive CO evolution as detected during C_3H_6-TPR experiments (Fig. 5a–d). However, further characterization will be conducted in order to well clarify this point.

To summarize, based on our previous results on methane oxidation over Co*x*Ce mixed oxides [32], an explanation of the different behaviour is attempted. We have reported for Co30Ce catalytic performance comparable to pure Co_3O_4 and an improvement of the methane oxidation activity with respect to samples with higher cobalt content, Co70Ce and Co50Ce. The superior performance obtained for the sample Co30Ce, having a Co/Ce atomic ratio equal to 1, was explained in terms of improved textural and reduction properties of Co_3O_4 induced by ceria [32,33].

With respect to the oxidation of methane, it is generally accepted that Co^{2+} ions in tetrahedral and Co^{3+} ions in octahedral coordination positions are active centres for adsorption of oxygen and hydrocarbons, respectively, [50–52]. Accordingly, Co*x*Ce perform better than CeO_2. Moreover, as methane cannot be easily oxidized, its oxidation does not start until 300 °C. Such a temperature is sufficiently high to involve bulk oxygen. Accordingly, a correlation between methane oxidation activity and redox properties was found for all the samples investigated, ceria included [32].

In the case of more reactive propene, the reaction takes place at much lower temperature and, depending on the nature of catalyst oxide one or two pathways can occur: at the surface of ceria the reaction involves only electrophilic oxygen species derived from gaseous oxygen filling surface vacancies; over Co*x*Ce oxides, both species, electrophilic oxygen and lattice oxygen may participate in the reaction depending on the temperature.

4. Conclusions

The present results demonstrate that complete propene oxidation can be achieved over Co_3O_4–CeO_2 mixed oxides below 350 °C, the most active samples giving full conversion of the hydrocarbon at 250 °C. As an important property, the catalysts maintain stable activity upon three consecutive heating–cooling cycles and unchanged textural and reduction properties. Among the Co*x*Ce series, Co30Ce exhibits the best activity giving at low-temperature propene conversion comparable to Co_3O_4.

SEM investigations of Co*x*Ce samples evidenced Co_3O_4 formation over sliver-shaped CeO_2 particles. This peculiar morphology could be a consequence of the calcination process, at 650 °C, driving the cobalt from the bulk to the surface. However, the average percentages of Co and Ce in the Co*x*Ce samples were quite homogeneous and close to the nominal ones.

Propene oxidation over pure CeO_2 requires, at low temperature, easily available oxygen species filling the surface oxide vacancies,

as shown by O_2-TPD curves. Moreover, also Co30Ce and, to a less extent, Co_3O_4 showed relevant concentration of surface oxygen species, likely involved in the propene oxidation.

On the other hand, for Co*x*Ce samples, the participation of bulk oxygen was evidenced by C_3H_6-TPR experiments. The higher activity of Co_3O_4 and Co30Ce with respect to the remaining Co*x*Ce samples was attributed to their higher mobility of lattice oxygen reacting with propene to form CO_2.

TPD experiments carried out after reaction at low conversion (10%) evidenced that no desorption of C_3H_6 and CO neither of carbonaceous species occurred, suggesting that C_3H_6, once adsorbed over the catalyst surface, is completely oxidized into CO_2 and water.

Acknowledgement

Bilateral project CNR-CNRS (2006–2007) is gratefully acknowledged for financial support.

References

[1] M. Amann, M. Lutz, J. Hazard. Mater. 78 (2000) 41.
[2] Environmental Fact Sheet No. 19, January 2006, produced by The Swedish NGO Secretariat on Acid Rain, Göteborg, Sweden.
[3] P. Le Cloirec, *Les composés organiques volatils dans l'environnement*, Technique et Documentation Lavoisier, Paris, 1998.
[4] P.O. Thevenin, A.G. Ersson, H.M.J. Kušar, P.G. Menon, S.G. Järås, Appl. Catal. A: Gen. 212 (2001) 189.
[5] M.F.M. Zwinkels, S.G. Järås, P.G. Menon, T.A. Griffin, Catal. Rev. Sci. Eng. 35 (1993) 319.
[6] R. Spinicci, M. Faticanti, P. Marini, S. De Rossi, P. Porta, J. Mol. Catal. A: Chem. 197 (2003) 147.
[7] M. Alifanti, M. Florea, S. Somacescu, V.I. Parvulescu, Appl. Catal. B: Environ. 60 (2005) 33.
[8] B.P. Barbero, J.A. Gamboa, L.E. Cadús, Appl. Catal. B: Environ. 65 (2006) 21.
[9] M. Labari, S. Siffert, J.-F. Lamonier, E.A. Zhilinskaya, A. Aboukaïs, Appl. Catal. B: Environ. 43 (2003) 261.
[10] M. Baldi, E. Finocchio, F. Milella, G. Busca, Appl. Catal. B: Environ. 16 (1998) 43.
[11] T. Ataloglou, J. Vakros, K. Bourikas, C. Fountzoula, C. Kordulis, A. Lycourghiotis, Appl. Catal. B: Environ. 57 (2005) 299.
[12] M. Shelef, K. Otto, H. Gandhi, J. Catal. 12 (1968) 361.
[13] Y.-F. Yu Yao, J. Catal. 33 (1974) 108.
[14] G.K. Boreskov, in: J.R. Anderson, M. Boudart (Eds.), Catalysis, Science and Technology, vol. 3, Springer Verlag, New York, 1982.
[15] H.-K. Lin, C.-B. Wang, H.-C. Chiu, S.-H. Chien, Catal. Lett. 86 (2003) 63.
[16] H.-K. Lin, H.-C. Chiu, H.-C. Tsai, S.-H. Chien, C.-B. Wang, Catal. Lett. 88 (2003) 169.
[17] C.-B. Wang, C.-W. Tang, S.-J. Gau, S.-H. Chien, Catal. Lett. 101 (2005) 59.
[18] F. Wyrwalski, J.-F. Lamonier, M.J. Perez-Zurita, S. Siffert, A. Aboukaïs, Catal. Lett. 108 (2006) 87.
[19] F. Wyrwalski, J.-F. Lamonier, S. Siffert, A. Aboukaïs, Appl. Catal. B: Environ. 70 (2007) 393.
[20] F. Wyrwalski, J.-F. Lamonier, S. Siffert, L. Gengembre, A. Aboukaïs, Catal. Today 119 (2007) 332.
[21] Y.-Z. Wang, Y.-X. Zhao, C.-G. Gao, D.-S. Liu, Catal. Lett. 116 (2007) 136.
[22] D. Terribile, A. Trovatelli, C. de Leitenburg, A. Primavera, G. Dolcetti, Catal. Today 47 (1999) 133.
[23] J. Kirchnerova, M. Alifanti, B. Delmon, Appl. Catal. A: Gen. 231 (2002) 65.
[24] G. Deganello, F. Giannici, A. Martorana, G. Pantaleo, A. Prestianni, A. Balerna, L.F. Liotta, A. Longo, J. Phys. Chem. B 110 (2006) 8731.
[25] W. Liu, M. Flytzani-Stephanopoulos, J. Catal. 153 (1995) 304.
[26] M. Kang, M.W. Song, C.H. Lee, Appl. Catal. A: Gen. 251 (2003) 143.
[27] M.M. Natile, A. Glisenti, Chem. Mater. 17 (2005) 3403.
[28] C. Li Xue, H. Zhang, Y. He, Teraoka, Appl. Catal. B: Environ. 75 (2007) 167.
[29] J.-Y. Luo, M. Meng, X. Li, X.-G. Li, Y.-Q. Zha, T.-D. Hu, Y.-N. Xie, J. Zhang, J. Catal. 254 (2008) 310.
[30] C.-W. Tang, C.-C. Kuo, M.-C. Kuo, C.-B. Wang, S.-H. Chien, Appl. Catal. A: Gen. 309 (2006) 37.
[31] C.-W. Tang, W.-Y. Yu, C.-J. Lin, C.-B. Wang, S.-H. Chien, Catal. Lett. 116 (2007) 161.
[32] L.F. Liotta, G. Di Carlo, G. Pantaleo, A.M. Venezia, G. Deganello, Appl. Catal. B: Environ. 66 (2006) 217.
[33] L.F. Liotta, G. Di Carlo, G. Pantaleo, G. Deganello, Appl. Catal. B: Environ. 70 (2007) 314.
[34] H. Fontane, M. Veillerot, J.C. Gallo, R. Guillermo, in: Proceedings of the 8th International Symposium on Transport and Air Pollution, Graz, 1999.
[35] E. Rivière, CITEPA Report, Paris, 1998.
[36] Inorganic Crystal Structure Data Base (ICSD), National Institute of Standards and Technology (NIST), release 2004/2.
[37] H.P. Klug, L.E. Alexander, X-ray Diffraction Procedures for Polycrystalline and Amorphous Materials, Wiley, New York, 1954.
[38] P. Denton, A. Giroir-Fendler, H. Praliaud, M. Primet, J. Catal. 189 (2000) 410.
[39] Y. Moro-oka, W. Ueda, K.-H. Lee, J. Mol. Catal. A: Chem. 199 (2003) 139.
[40] R.J.H. Voorhoeve, J.P. Remeika, D.W. Johnson, Science 180 (1973) 62.
[41] Y. Teraoka, M. Yoshimatsu, N. Yamazoe, T. Seiyama, Chem. Lett. (1984) 893.
[42] H.M. Zhang, Y. Shimizu, Y. Teraoka, N. Miura, N. Yamazoe, J. Catal. 121 (1990) 432.
[43] J.L.G. Fierro, Catal. Today 8 (1990) 153.
[44] A. Trovarelli, Catalysis by Ceria and Related Materials, Imperial College Press, London, 2002.
[45] C. Binet, M. Daturi, J.-C. Lavalley, Catal. Today 50 (1999) 207.
[46] J. Haber, in: B.K. Warren, S.T.. Oyama (Eds.), Proceedings Symposium Heterogeneous Hydrocarbon Oxidation, ACS Symposium Series, vol. 638, American Chemical Society, Washington, DC, 1996, p. 20.
[47] J. Haber, Studies Surface Science Catalysis, vol. 110, Elsevier, Amsterdam, 1997, p. 1.
[48] J. Haber, W. Turek, J. Catal. 190 (2000) 320.
[49] G.K. Boreskov, Catalysis: Science and Technology, vol. 3, Springer Verlag, Berlin, 1982, p. 39.
[50] J. Łojewska, A. Kołodziej, J. Żak, J. Stoch. Catal. Today 105 (2005) 655.
[51] R.S. Drago, K. Jurczyk, D.J. Singh, V. Young, Appl. Catal. B: Environ. 6 (1995) 155.
[52] V.G. Milt, M.A. Ulla, E.A. Lombardo, Catal. Lett. 65 (2000) 67.